Electronic Supplementary Material (ESI) for Chemical Communications.

Supplementary Information

Long life of exceeding 10000 Cycles aluminum-ion batteries based on FeTe$_2$@GO composite as cathode

Li Yang,[a] Jie Liu,[a] Yongshuai Liu,[a] Yuhao Li,[a] Fengkai Zuo,[a] Yifei Xu,[a] Yangyang Wu,[a] Qiang Li[a] and Hongsen Li*[a]

[a] College of Physics, Center for Marine Observation and Communications, Qingdao University, Qingdao 266071, P. R. China.

* Correspondence authors: hsli@qdu.edu.cn

Experimental section

Materials.

Ammonium iron(II) sulfate hexahydrate ($(NH_4)_2Fe(SO_4)_2\cdot6H_2O$, 99.5%), sodium hydroxide (NaOH, 96%), hydrazinium hydrate ($N_2H_4\cdot H_2O$, 80%), tellurium (Te, 99.99%) were purchased from Aladdin Reagent. Polyvinylidene fluoride (PVDF) binder and N-methyl-2-pyrrolidone (NMP) were provided by Shenzhen KejingStar Technology. Propylene carbonate (PC, 99.95%), aluminium chloride/1ethyl-3-methylimidazolium chloride ($AlCl_3$/[EMIm]Cl) and Whatman GF/C type glass fiber were provided by Dodochem. All chemicals are analytical grade without further purification.

Synthesis of pure $FeTe_2$.

The $FeTe_2$ nanocrystals were synthesized *via* a traditional hydrothermal method. In a typical synthesis, 20 mL of $(NH_4)_2Fe(SO_4)_2\cdot6H_2O$ (0.1 M) and 15 mL of NaOH (1 M) were mixed to get a new solution, and then 4 mL of $N_2H_4\cdot H_2O$ was injected dropwise into this solution with continuous stirring for 20 min at room temperature to obtain a brown suspension. 3.6 mmol of Te powder was added to the brown suspension and the mixture was sonicated for 30 min. Whereafter, the mixture was transferred to 80 mL Teflon-lined autoclave to heat at 180 °C for 14 h. After cooling to room temperature, the material was centrifuged and washed several times with deionized water and absolute ethanol. The final $FeTe_2$ nanocrystal powder was collected *via* vacuum drying at 60 °C overnight.

Synthesis of $FeTe_2$@GO.

10 mg of GO was added into 20 mL of deionized water and sonicated for 2 h. Subsequently 20 mg of $FeTe_2$ was dispersed into 20 mL deionized water with stirring for 20 min, and then, the GO suspension was added to $FeTe_2$ solution and mixed well. Finally, the $FeTe_2$@GO was obtained after the mixture was centrifuged, washed and dried at 60 °C for 14 h.

Materials characterization.

X-ray diffraction (XRD, Bruker D8 advance) with a Cu *K*α radiation was implemented in order to determine the phase compositions. The microstructures of sample were explored by field-emission scanning electron microscopy (FESEM, ZEISS, Sigma 300) as well as transmission electron microscope (TEM, JEOL, JEM-2100F). The chemical state of composite and the element distribution were investigated by X-ray photoelectron spectroscopy (XPS, ESCALAB250Xi) and energy dispersive spectrometer (EDS, ZEISS, Sigma 500). Raman spectra on a LabRAM HR Evolution Raman spectrometer (HORIBA JY) was also measured.

Electrochemical measurements.

The aluminum-ion storage properties of the $FeTe_2$@GO were measured by punch cells. First, active material, conductive carbon black (Super P) and binder of polyvinylidene fluoride (PVDF) were mixed with a weight proportion 7:2:1 in dispersant of N-methyl-pyrrolidone (NMP) to obtain the required slurry. And then, it was coated on metal molybdenum sheet and dried at 60 °C overnight under vacuum. Lastly, the battery that aluminum foils as anode, the ionic liquid of $AlCl_3$/[EMIm]Cl with a 1.3:1 molar ratio as electrolyte, Whatman GF/C type glass fiber as separator, and prepared $FeTe_2$@GO cathode were assembled in a glove box with the argon atmosphere. The galvanostatic discharge/charge profiles of the self-assembly AIBs was measured using CT2001A LAND test system. Cyclic voltammetry (CV) measurements were performed employing electrochemical workstation (Chenhua Instrument, CHI 660D). All of the specific capacities obtained are based on the mass of cathode active materials.

Computational methods.

All the calculations were implemented under the architecture framework of the density functional theory (DFT) as applied in the Vienna ab initio Software Package code, which was operated in the Perdew-Burke-Ernzerhof (PBE) generalized gradient approximation and the projected augmented wave (PAW) method. It is based on a 2×2×1 supercell which can prevent adsorbate ions from the interaction with its images in neighboring supercells. The setting of cut-off energy of the plane-wave basis was intended to 450 eV. The convergence criterion for the electronic self-consistent iteration and force was set to 10^{-5} eV and 0.01 eV $Å^{-1}$, respectively. Apart from that, a high binding energy site is adopted when consider of the orthorhombic symmetry, making sure the stable configuration of the insertion of ions within the $FeTe_2$ lattice. The formation energy (E_b) of different intercalated ions can be figured out through the following formula:

$$E(b) = E(Total) - E(FeTe_2) - E(Al_xCl_y)$$

where E(Total) is the total energies of whole system with inserted ions, $E(FeTe_2)$ and $E(Al_xCl_y)$ represent the energy of single $FeTe_2$ supercell and single inserted ions, respectively.

Supporting Figures:

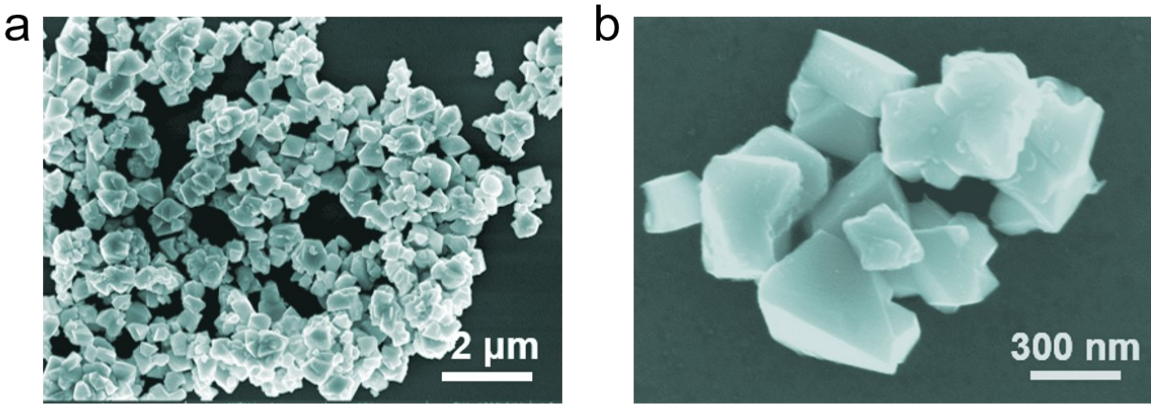

Figure S1. The FESEM images of $FeTe_2$ with different magnification.

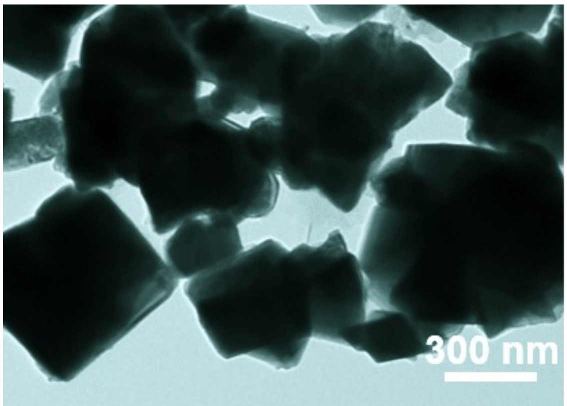

Figure S2. The TEM images of $FeTe_2$.

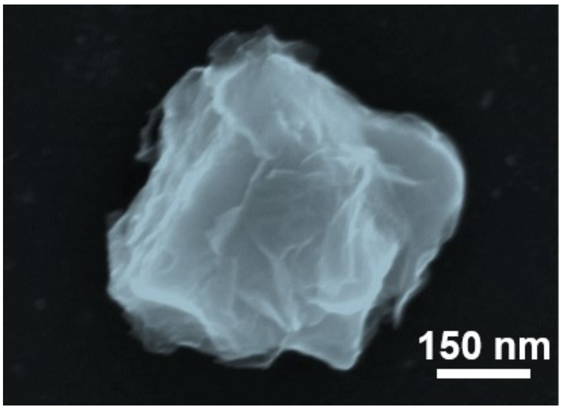

Figure S3. The FESEM images of $FeTe_2$@GO.

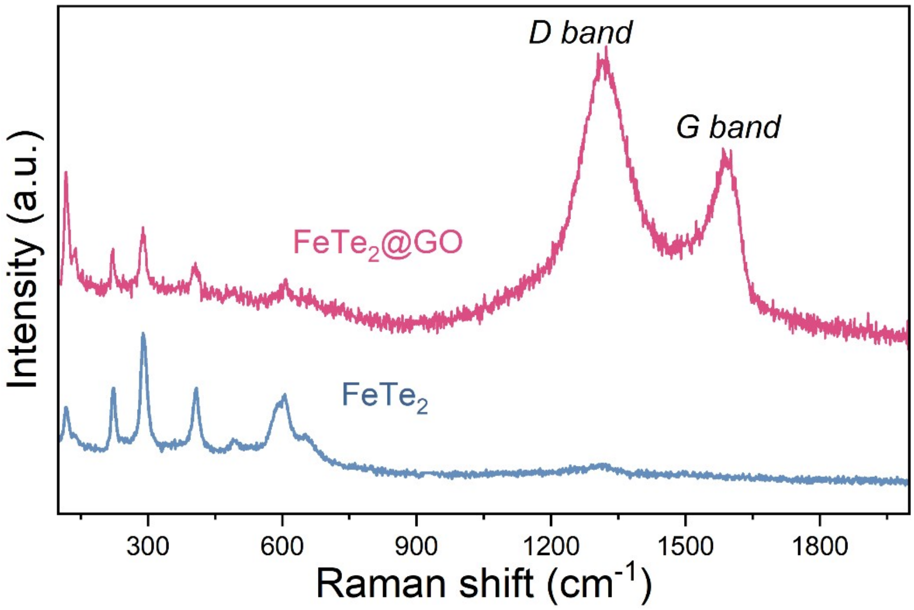

Figure S4. Raman spectra of $FeTe_2$ and $FeTe_2$@GO.

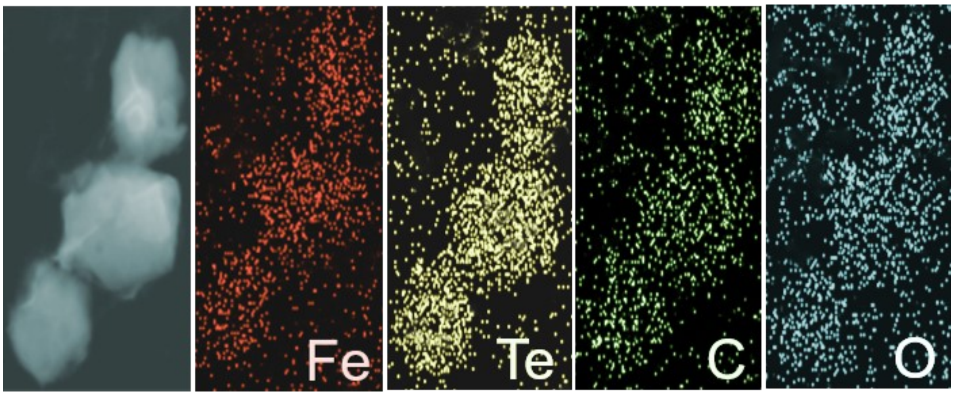

Figure S5. EDS mapping of $FeTe_2$@GO.

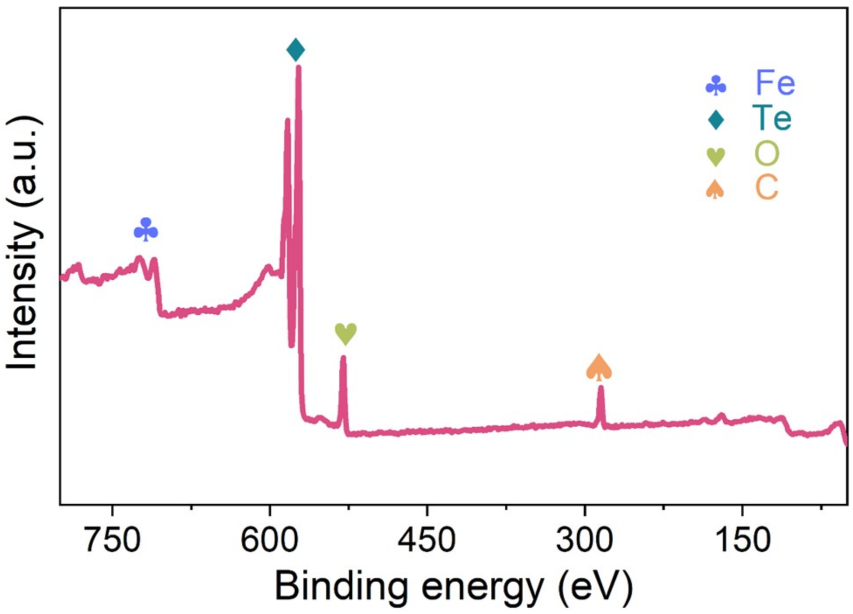

Figure S6. Full-scan XPS spectrum of $FeTe_2$.

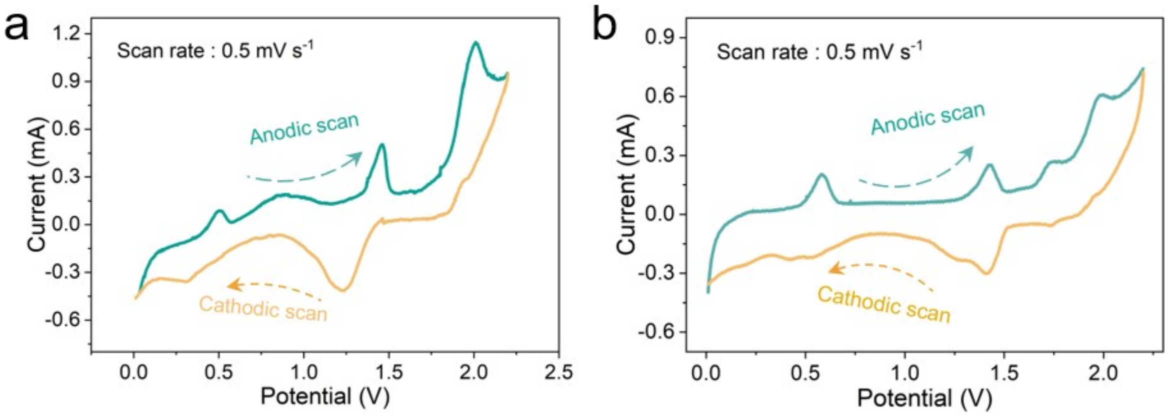

Figure S7. CV curves for (a) the $FeTe_2$ electrode and (b) $FeTe_2$@GO electrode.

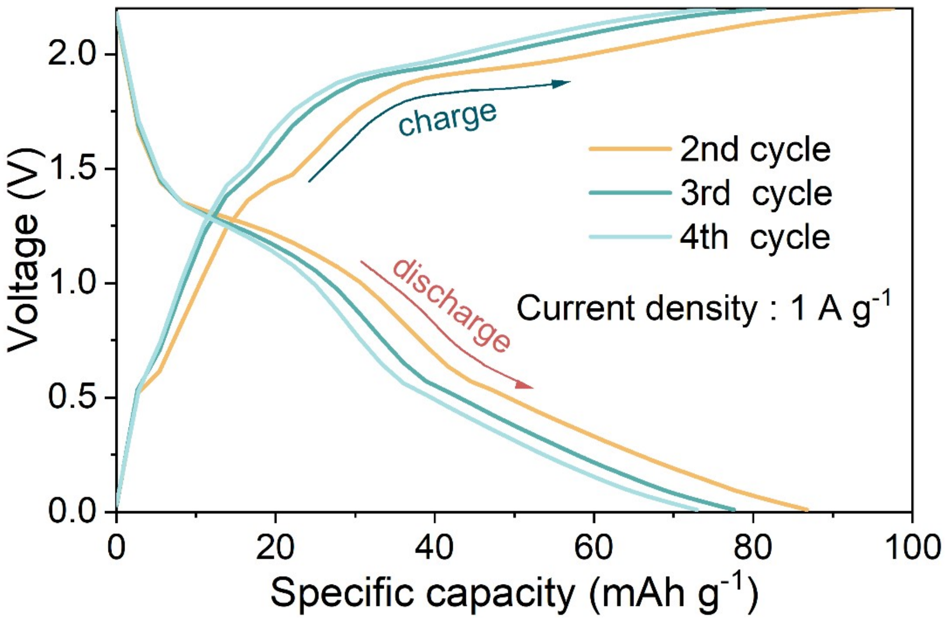

Figure S8. Charge/discharge curves of $FeTe_2$ at a current density of 1 A g^{-1}.

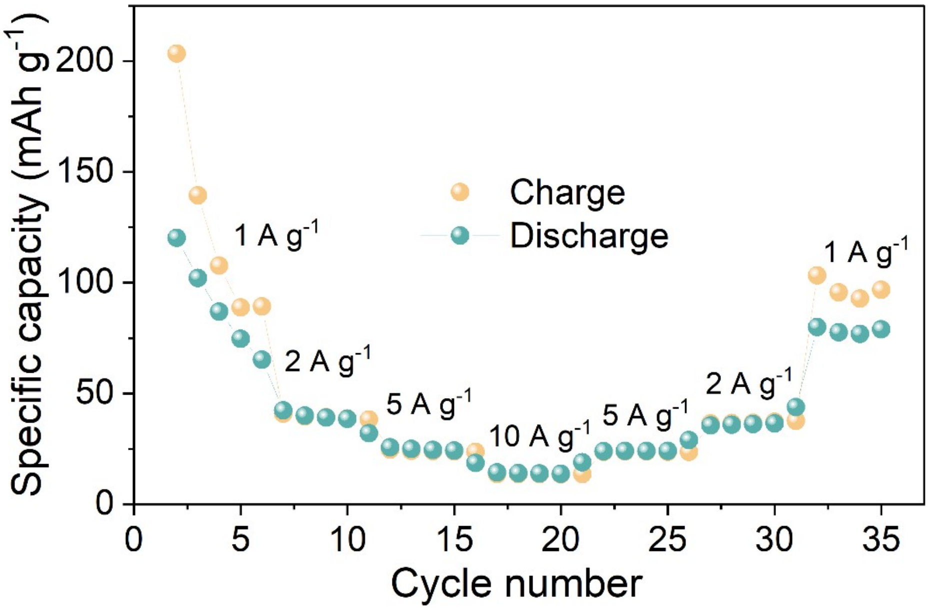

Figure S9. Rate performance under different current densities from 1 to 10 A g^{-1} of $FeTe_2$.

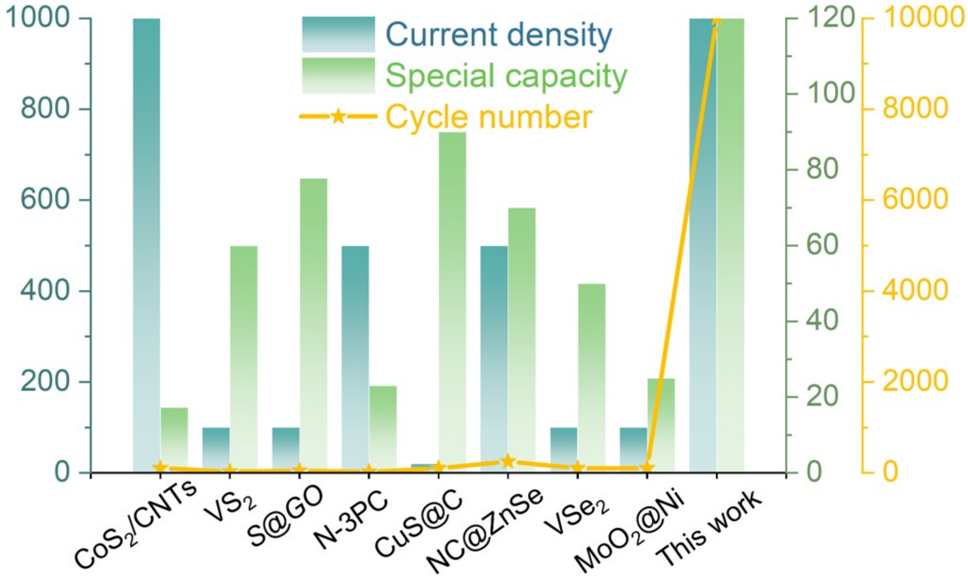

Figure S10. The comparison of capacity (unit: mA h g^{-1}), current densities (unit: mA g^{-1}), versus cycle number of the $FeTe_2$@GO electrode with various reported research electrodes for AIBs.

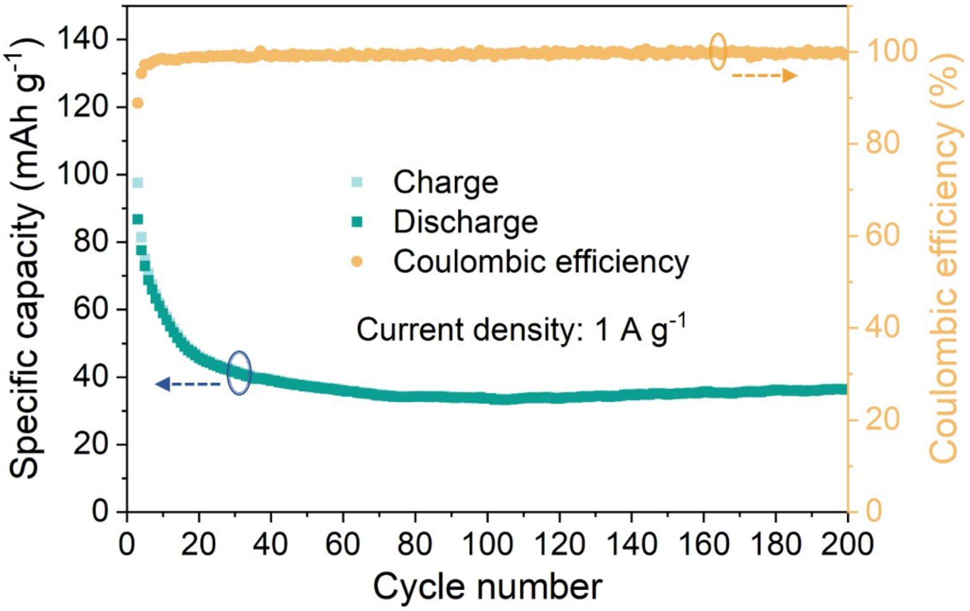

Figure S11. Cycling stability of $FeTe_2$ at a current density of 1 A g^{-1}.

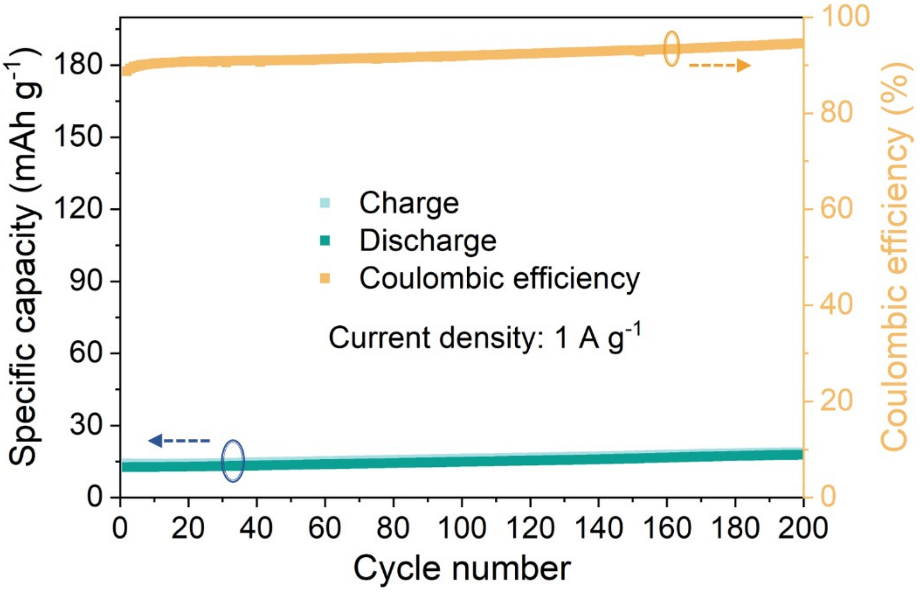

Figure S12. Cycling performance of GO at a current density of 1A g^{-1}.

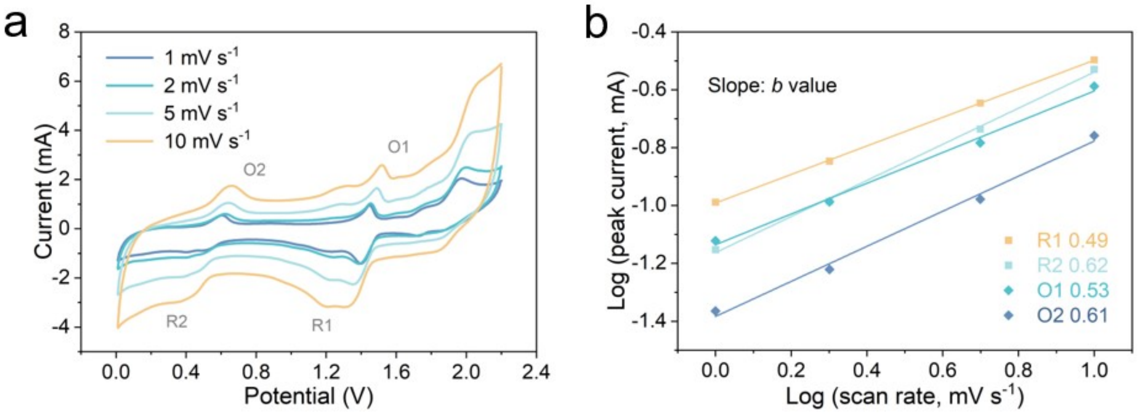

Figure S13. CV curves at different scan rates (a), *b* value (b) of $FeTe_2$@GO electrode.

The CV measurements of $FeTe_2$@GO were operated at different scan rates (1, 2, 5, 10 mV s^{-1}) to investigate the kinetics of the electrodes of $FeTe_2$@GO Noted that the redox peaks shift mildly with increasing scanning rate, manifesting high reversibility of the $FeTe_2$@GO cathodes with minor polarization.[1] The peak currents (i) and scan rates (v) in CV curves comply with the power-law relationship ($i = av^b$) in which a and b are adjustable parameters.[2] Index b is of considerable importance to probe into kinetic behavior of the battery and it could be predicated by the slope of log (i) versus log (v) plot.[3] As shown in the fitting curve (Fig. 2h), the fitted slope b values of peak R1, peak R2, peak O1 and peak O2 are calculated to be 0.49, 0.62, 0.53 and 0.61, and there are quite close to 0.5 which mainly corresponded to a diffusion-controlled process.[4]

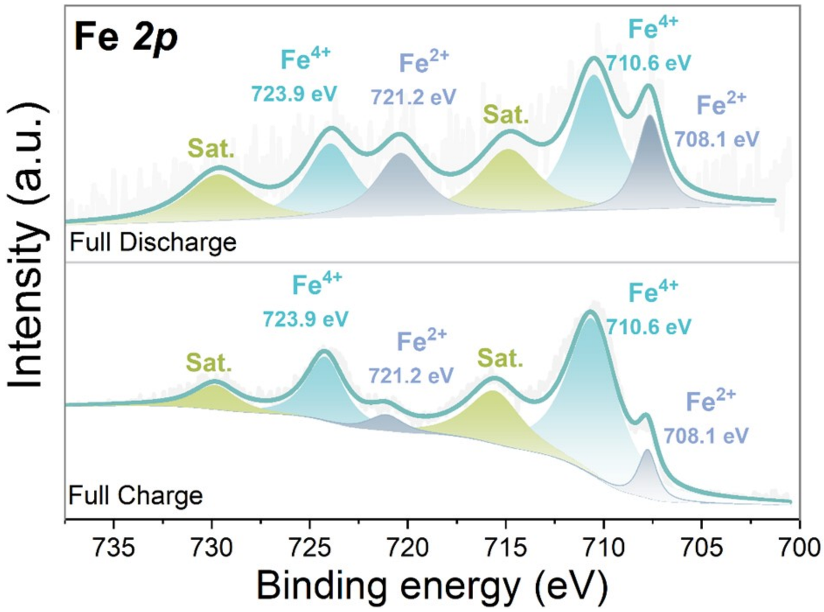

Figure S14. The Fe 2*p* XPS spectra of $FeTe_2$@GO for the second cycle.

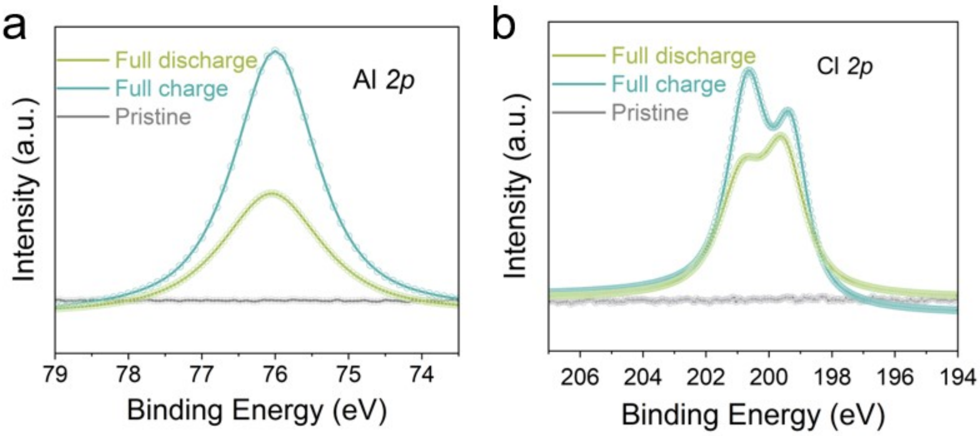

Figure S15. (a) Al 2*p* and (b) Cl 2*p* XPS spectra at the state of pristine, fully charged and fully discharged for the first cycle, respectively.

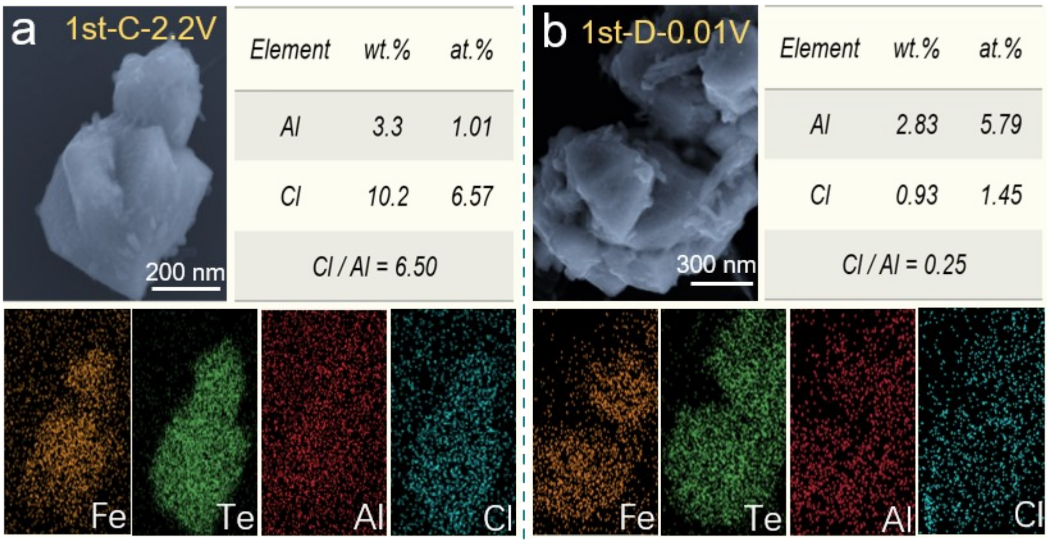

Element	*wt.%*	*at.%*
Al	*3.3*	*1.01*
Cl	*10.2*	*6.57*
Cl / Al = 6.50		

Element	*wt.%*	*at.%*
Al	*2.83*	*5.79*
Cl	*0.93*	*1.45*
Cl / Al = 0.25		

Figure S16. Elemental mapping analysis of the FeTe$_2$ electrode at charge to 2.2 V (a), discharge to 0.01 V (b).

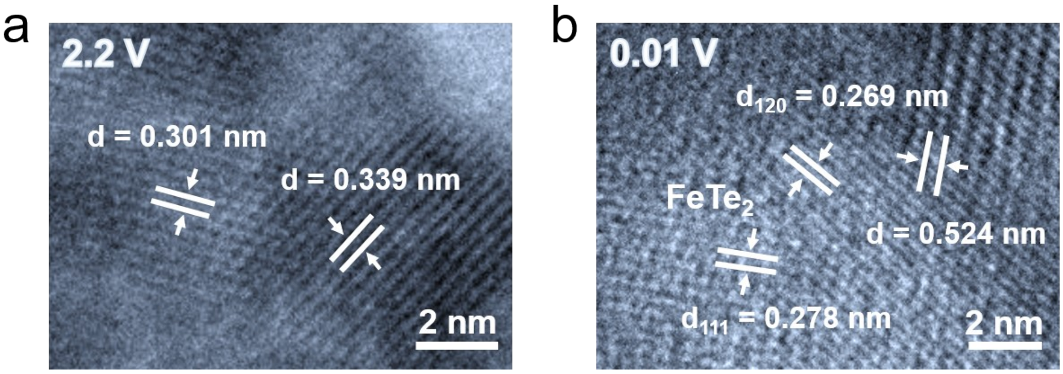

Figure S17. HRTEM images of $FeTe_2$ when charged to 2.2 V (a) and discharged to 0.01 V (b).

The internal lattice spacing for the charged product was measured and two groups of lattice spacings appeared to have expanded, which could be ascribed to the formation of $Fe(AlCl_4)_mTe_2$ and $FeCl_nTe_2$ (Fig. S17(a)). The sample in the discharged state presented three sets of internal lattice spacings (Fig. S17(b)): lattice fringes having interplanar spacings of 0.278 nm and 0.269 nm, corresponding to the (111) and (120) lattice planes of the $FeTe_2$ crystal; and an extended lattice spacing of up to 0.524 nm, due to the formation of Al_xFeTe_2.

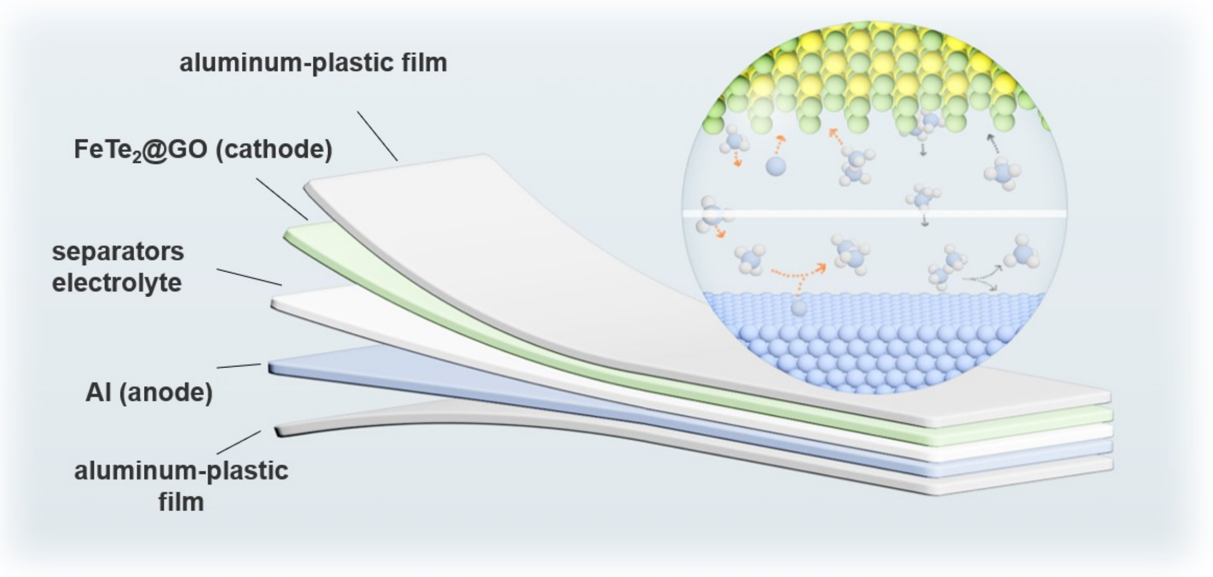

Figure S18. Schematic illustration of the structure of the $FeTe_2$@GO//Al pouch-type battery.

Table S1. Comparison of some typical cathode materials for AIBs.

Type of materials	**Cycle number**	**Current density (mA g^{-1})**	**Special capacity (mAh g^{-1})**	**Ref.**
MoO_2@Ni	100	100	25.0	[5]
VSe_2	100	100	50.0	[6]
NC@ZnSe	250	500	70.0	[7]
CuS@C	100	20	90.0	[8]
N-3PC	20	500	23.0	[9]
S@GO	50	100	77.8	[10]
VS_2	30	100	60.0	[11]
CoS_2@CNTs	100	1000	17.3	[12]
$FeTe_2$@GO	**10000**	**1000**	**120.4**	**This work**

Table S2. Cathode materials and the corresponding charge carriers for AIBs.

Type of materials	Charge carriers	Ref.
VS_2	Al^{3+}	11
VS_4	Al^{3+}	13
FeS_2	Al^{3+}	14
CoS_2	Al^{3+}	12
Co_3S_4	Al^{3+}	15
Ni_3S_2	Al^{3+}	16
CuS	Al^{3+}	8
MoS_2	Al^{3+}	17
WS_2	$AlCl_4^-$	18
$FeSe_2$	Al^{3+}, Cl^-, $AlCl_4^-$	19
$CoSe_2$	Al^{3+}	20
$NiSe_2$	$AlCl_4^-$, Cl^-	21
$ZnSe_2$	Al^{3+}	7
$MoSe_2$	Al^{3+}, $AlCl_4^-$	22
$CoTe_2$	$AlCl_4^-$	23
NiTe	$AlCl_4^-$	24
$FeTe_2$	**Al^{3+}, $AlCl_4^-$, Cl^-**	**This work**

References

1 Y. Hu, H. Huang, D. Yu, X. Wang, L. Li, H. Hu, X. Zhu, S. Peng and L. Wang, *Nanomicro Lett.*, 2021, **13,** 159.

2 Q. Li, H. Li, Q. Xia, Z. Hu, Y. Zhu, S. Yan, C. Ge, Q. Zhang, X. Wang, X. Shang, S. Fan, Y. Long, L. Gu, G. Miao, G. Yu and J. S. Moodera, *Nat. Mater.*, 2021, **20,** 76-83.

3 S.-K. Jung, H. Kim, M. G. Cho, S.-P. Cho, B. Lee, H. Kim, Y.-U. Park, J. Hong, K.-Y. Park, G. Yoon, Won M. Seong, Y. Cho, Myoung H. Oh, H. Kim, H. Gwon, I. Hwang, T. Hyeon, W.-S. Yoon and K. Kang, *Nat. Energy,* 2017, **2,** 16208.

4 N. Feng, R. Meng, L. Zu, Y. Feng, C. Peng, J. Huang, G. Liu, B. Chen and J. Yang, *Nat. Commun.,* 2019, **10,** 1372.

5 J. Wei, W. Chen, D. Chen and K. Yang, J. *Electrochem. Soc.*, 2017, **164,** A2304-A2309.

6 H. Lei, M. Wang, J. Tu and S. Jiao, *Sustainable Energy Fuels,* 2019, **3,** 2717-2724.

7 J. Li, W. Liu, Z. Yu, J. Deng, S. Zhong, Q. Xiao, F. chen and D. Yan, *Electrochim. Acta,* 2021, **370,** 137790.

8 S. Wang, S. Jiao, J. Wang, H. S. Chen, D. Tian, H. Lei and D. N. Fang, *ACS Nano,* 2017, **11,** 469-477.

9 J. Xu, P. Jiang, X. Liang, R. Tian and Y. Liu, *Fullerenes Nanotub. Carbon Nanostructures*, 2020, **29,** 21-27.

10 K. Zhang, T. H. Lee, J. H. Cha, H. W. Jang, M. Shokouhimehr and J.-W. *Choi, Electron. Mater. Lett.,* 2019, **15,** 720-726.

11 L. Wu, R. Sun, F. Xiong, C. Pei, K. Han, C. Peng, Y. Fan, W. Yang, Q. An and L. Mai, *Phys. Chem. Chem. Phys.,* 2018, **20,** 22563-22568.

12 R. Zhuang, Z. Huang, S. Wang, J. Qiao, J.-C. Wu and J. Yang, *Chem. Eng. J.,* 2021, **409,** 128235.

13 L. Xing, K. A. Owusu, X. Liu, J. Meng, K. Wang, Q. An and L. Mai, *Nano Energy,* 2021, **79,** 105384.

14 T. Mori, Y. Orikasa, K. Nakanishi, C. Kezheng, M. Hattori, T. Ohta and Y. Uchimoto, *J. Power Sources,* 2016, **313,** 9-14.

15 H. Li, H. Yang, Z. Sun, Y. Shi, H.-M. Cheng and F. Li, *Nano Energy,* 2019, **56,** 100-108.

16 S. Wang, Z. Yu, J. Tu, J. Wang, D. Tian, Y. Liu and S. Jiao, *Adv. Energy Mater.*, 2016, **6,** 1600137.

17 Z. Li, B. Niu, J. Liu, J. Li and F. Kang, *ACS Appl Mater Interfaces,* 2018, **10,** 9451-9459.

18 Z. Zhao, Z. Hu, Q. Li, H. Li, X. Zhang, Y. Zhuang, F. Wang and G. Yu, *Nano Today,* 2020, **32,** 100870.

19 H. Wang, L. Zhao, H. Zhang, Y. Liu, L. Yang, F. Li, W. Liu, X. Dong, X. Li, Z. Li, X. Qi, L. Wu, Y. Xu, Y. Wang, K. Wang, H. Yang, Q. Li, S. Yan, X. Zhang, F. Li and H. Li, *Energy Environ. Sci.,* 2022, **15,** 311-319.

20 T. Cai, L. Zhao, H. Hu, T. Li, X. Li, S. Guo, Y. Li, Q. Xue, W. Xing, Z. Yan and L. Wang, *Energy Environ. Sci.,* 2018, **11,** 2341-2347.

21 H. Zhang, Y. Liu, L. Yang, L. Zhao, X. Dong, H. Wang, Y. Li, T. Sun, Q. Li and H. Li, *Energy Storage Mater.,* 2022, **47,** 336-344.

22 Y. Ai, S. Wu, K. Wang, T. Yang, M. Liu, H. Liao, J. Sun, J. Chen, S. Tang, D. Wu, T. Su, Y. Wang, H. Chen, S. Zhang, W. Liu, Y. Chen, L. Lee, J. He, Z. Wang and Y. Chueh, *ACS Nano,* 2020, **14,** 8539-8550.

23 B. Zhang, Y. Zhang, J. Li, J. Liu, X. Huo and F. Kang, *J. Mater. Chem. A,* 2020, **8,** 5535-5545.

24 Z. Yu, S. Jiao, J. Tu, Y. Luo, W. Song, H. Jiao, M. Wang, H. Chen and D. Fang, *ACS Nano,* 2020, **14,** 3469-3476.